J|A|C|S
ARTICLES
Published on Web 04/13/2004

Exploring the Electronic and Mechanical Properties of Protein Using Conducting Atomic Force Microscopy

Jianwei Zhao,[†] Jason J. Davis,*[,†] Mark S. P. Sansom,[‡] and Andrew Hung[‡]

Contribution from the Inorganic Chemistry Laboratory, Department of Chemistry, South Parks Road, Oxford, OX1 3QR; Bionanotechnology IRC, Clarendon Laboratory, Department of Physics, University of Oxford, Parks Road, Oxford OX1 3PU, and Laboratory of Molecular Biophysics, Department of Biochemistry, University of Oxford, South Parks Road, OX1 3QU United Kingdom

Received November 3, 2003; E-mail: Jason.davis@chem.ox.ac.uk

Abstract: In interfacing man-made electronic components with specifically folded biomacromolecules, the perturbative effects of junction structure on any signal generated should be considered. We report herein on the electron-transfer characteristics of the blue copper metalloprotein, azurin, as characterized at a refined level by conducting atomic force microscopy (C-AFM). Specifically, the modulation of current−voltage (I−V) behavior with compressional force has been examined. In the absence of assignable resonant electron tunneling within the confined bias region, from −1 to 1 V, the I−V behavior was analyzed with a modified Simmons formula. To interpret the variation of tunneling barrier height and barrier length obtained by fitting with the modified Simmons formula, an atom packing density model associated with protein mechanical deformation was proposed and simulated by molecular dynamics. The barrier heights determined at the minimum forces necessary for stable electrical contact correlate reasonably well with those estimated from bulk biophysical (electroanalytical and photochemical) experiments previously reported. At higher forces, the tunnel barrier decreases to fall within the range observed with saturated organic systems. Molecular dynamics simulations revealed changes in secondary structure and atomic density of the protein with respect to compression. At low compression, where transport measurements are made, secondary structure is retained, and atomic packing density is observed to increase linearly with force. These predictions, and those made at higher compression, are consistent with both experimentally observed modulations of tunneling barrier height with applied force and the applicability of the atom packing density model of electron tunneling in proteins to molecular-level analyses.

Introduction

Understanding the processes associated with protein-based electron transfer is of fundamental importance in both the life sciences, and the potential exploitation of new biomolecular electronic devices.[1] Of those techniques which have been utilized in the study of the electron-transfer protein electronics, those based on photochemistry,[2] electrochemistry,[3] and, more recently, molecular junctions,[1,4] have been, perhaps, the most fruitful. The high spatial resolution associated with a Scanning Tunneling Microscope (STM)[5] has been exploited in the tunneling analysis of protein at a molecular level.[1,3,6] Though such experiments are demonstrably powerful, in the sense of resolving molecular density of states (DOS), the location of the tunneling tip with respect to the molecule of interest is, essentially, unknown. In the nondestructive acquisition of tunneling images, junction resistances are typically set to a giga-ohm (GΩ) level, during which the tip is likely to reside above the surface-confined molecule.[3,6]

To control both junction electrical contact and mechanical perturbation of the structure of interest, the force feedback inherent in conductive-probe AFM (C-AFM) can be utilized.[7] In a C-AFM measurement, a metal-coated tip, several tens of nm in radius, is maintained in mechanical contact with the

[†] Inorganic Chemistry Laboratory, Oxford.
[‡] Laboratory of Molecular Biophysics, University of Oxford.

(1) (a) Page, C. C.; Moser, C. C.; Chen, X.; Dutton, P. L. *Nature* **1999**, *402*, 47−52. (b) Jeuken, L. J. C.; McEvoy, J. P.; Armstrong, F. A. *J. Phys. Chem. B* **2002**, *106*, 2304−2313.(c) Davis, J. *Philos. Trans. Royal Soc. A* **2003**, in press. (d) Rinaldi, R.; Biasco, A.; Maruccio, G.; Arima, V.; Visconti, P.; Cingolani, R.; Facci, P.; Rienzo, F. D.; Felice, R. D.; Molinari, E.; Verbeet, M. P.; Canters, G. W. *Appl. Phys. Lett.* **2003**, *82*, 472−474.
(2) (a) Gray, H. B. *Proc. Natl. Acad. Sci. U.S.A.* **2003**, *100*, 3563−3568. (b) Pascher, T.; Chesick, J. P.; Winkler, J. R.; Gray, H. B. *Science* **1996**, *271*, 1558−1560.
(3) (a) Gaigalas, A. K.; Niaura, G. *J. Colloid. Interface. Sci.* **1997**, *193*, 60−70. (b) Chi, Q.; Zhang, J.; Andersen, J. E. T.; Ulstrup, J. *J. Phys. Chem. B* **2001**, *105*, 4669−4679. (c) Zhang, J.; Chi, Q.; Kuznetsov, A. M.; Hansen, A. G.; Wackerbarth, H.; Christensen, H. E. M.; Andersen, J. E. T.; Ulstrup, J. *J. Phys. Chem. B* **2002**, *106*, 1131−1152. (d) Davis, J. J.; Hill, H. A. O.; Bond, A. M. *Coord. Chem. Rev.* **2000**, *200*−*202*, 411.
(4) Zhao, J.; Davis, J. J. *Nanotechnology* **2003**, *14*, 1023−1028.
(5) Wiesendanger, R. *Scanning Probe Microscopy and Spectroscopy*; Cambridge University Press: Cambridge, 1994, chapter 1.
(6) (a) Davis, J. J.; Hill, H. A. O. *J. Chem. Soc. Chem. Commun.* **2002**, *5*, 393−401. (b) Friis, E. P.; Andersen, J. E. T.; Kharkats, Y. I.; Kuznetsov, A. M.; Nichols, R. J.; Zhang, J. D.; Ulstrup, J. *Proc. Natl. Acad. Sci. U.S.A.* **1999**, *96*, 1379−1384. (c) Lee, I.; Lee, J. W.; Warmack, R. J.; Allison, D. P.; Greenbaum, E. *Proc. Natl. Acad. Sci. U.S.A.* **1995**, *92*, 1965−1969. (d) Khomutov, G. B.; Belovolova, L. V.; Gubin, S. P.; Khanin, V. V.; Obydenov, A. Y.; Sergeev-Cherenkov, A. N.; Soldatov, E. S.; Trifonov, A. S. *Bioelectrochemistry* **2002**, *55*, 177−181.
(7) (a) Zhao, J.; Uosaki, K. *Nanoletters* **2002**, *2*, 137−140. (b) Zhao, J.; Uosaki, K. *Langmuir* **2001**, *17*, 7784−7788.

sample while conductivity measurements are carried out at a molecular level.[8] The piezoelectronic control within such experiments enables the force dependence of structural deformation to be resolved.[8,9]

The electron transfer through "model", structurally ordered, closely packed self-assembled monolayers (SAMs), has been widely studied by using C-AFM. Frisbie et al. studied the electron transfer through a series of alkanethiol SAMs on gold, and resolved an electron tunneling decay coefficient, β, of 1.15∼1.45 per methylene.[9] In related work under solvent, Lindsay et al. reported the effects of force and bias on molecular conductance and calculated a β value of 0.8 ± 0.2 per methylene over ±3 V range.[9] The decay parameters attainable from these experiments have been predictably smaller than those observed in vacum (2.8 $Å^{-1}$ to 3.5 $Å^{-1}$) and consistent with electroanalytical determinations.[9,10]

Several physical models have been applied to the theoretical analysis of electron tunneling across organic molecules. A simple treatment of the organic medium as a continuum barrier was originally proposed by Simmons[11] and has been successfully used in the interpretation of tunneling images[5] and molecular layer electron-transfer characteristics.[9,10,12] Within this framework current density, i, is expressed by eq 1

$$i = \frac{e^2}{2\pi h L^2}\left\{\left(\varphi_0 - \frac{V}{2}\right)\exp\left[-K\left(\varphi_0 - \frac{V}{2}\right)^{1/2}\right] - \left(\varphi_0 + \frac{V}{2}\right)\exp\left[-K\left(\varphi_0 + \frac{V}{2}\right)^{1/2}\right]\right\} \quad (1)$$

where

$$K = \frac{4\pi L}{h}(2me)^{1/2} \quad (2)$$

and L and φ_0 denote barrier length and mean barrier height respectively (other symbols having their usual meaning). The theoretical model proposed by Mujica and Ratner[12,13] incorporates molecular structure into the tunneling barrier in its consideration of off-resonance electron tunneling across a metal-molecule-metal junction. The assumptions made here are (i) that the molecules in the monolayer act independently, that is, the total current is the product of the current through a single molecule scaled to the molecular density, and (ii) that the electrostatic potential profile can be determined self-consistently through the combined solution of Poisson and Schrödinger equations.[13] This model leads to an approximately constant electrostatic potential in the molecular bridge region, while the voltage drop occurs at the electrode-molecule interface. The current density, i, through such junctions is given by eq 3

$$i = \frac{4e^{2-2N}}{h}\frac{n\Delta_0^{\,2}t^{2(N-1)}}{1-2N}\{(\varphi_0 + V/2)^{1-2N} - (\varphi_0 - V/2)^{1-2N}\} \quad (3)$$

where N is the number of sites that compose a homogeneous molecular bridge, t is the transfer integral between sites, Δ_0 is the spectral density of either of the two electrodes at zero bias, n is the number of molecules per unit area and ϕ is the energy difference between the Fermi level of the electrode and the potential energy (assumed to be constant) of the molecular bridge. Though differing in the degree to which molecular structure is considered, the Simmons and Mujica's models are numerically similar in their predictions.[10,12]

In this paper, we focus on the direct measurement and mechanical modulation of the electronic properties of the blue copper protein, azurin. This protein, which plays an important role in respiratory and photosynthetic electron transport chains, contains a surface disulfide (Cys3-Cys26) group opposite to the strongly asymmetrically located Cu-center (Figure 1a).[14] This group serves as an anchor in the formation of a stable monolayer on Au (111) with the Cu-center oriented away from the surface.[14,15] To study the force dependence of measured protein conductance, the molecule was trapped robustly between a conducting AFM probe and an underlying substrate using a tip modification procedure (Figure 1a). In the present study, highly oriented pyrolytic graphite (HOPG) is used as the substrate. In this configuration, interfacial frictional forces between the tip and surface are minimized; the electrode, at which this protein associates only weakly, is atomically flat.[4] To study the mechanics of this configuration, it is essential to know the dimensions of the protein under compression. Both the tunneling distance (i.e., the vertical dimension of protein) and the barrier height are derivable by fitting I−V curves to a Simmons expression. In its original form, however, this model predicts perfectly symmetrical current−voltage (I−V) behavior from which deviations, particularly at high force, are observed. In modifying the Simmons model through the incorporation of an asymmetric bias division, fits to experimental data are good and allow a determination of tunnel distance and, hence, protein vertical compression at specific load. From these data a deduction of "molecular Youngs modulus", in reasonable agreement with previous bulk determinations, can be made.

Furthermore, we have performed molecular dynamics (MD) simulations of azurin compression in order to investigate, at

(8) (a) Cui, X. D.; Primak, A.; Zarate, X.; Tomfohr, J.; Sankey, O. F.; Moore, A. L.; Moore, T. A.; Gust, D.; Harris, G.; Lindsay, S. M. *Science* **2001**, *294*, 571−574. (b) Ganesh, K.; Ramachandran, K.; Tomfohr, J. K.; Li, J.; Sankey, O. F.; Zarate, X.; Primak, A.; Terazono, Y.; Moore, T. A.; Moore, A. L.; Gust, D.; Nagahara, L. A.; Lindsay, S. M. *J. Phys. Chem. B* **2003**, *107*, 6162−6169. (c) Leatherman, G.; Durantini, E. N.; Gust, D.; Moore, T. A.; Moore, A. L.; Stone, S.; Zhou, Z.; Rez, P.; Liu, Y. Z.; Lindsay, S. M. *J. Phys. Chem. B* **1999**, *103*, 4006.

(9) (a) Beebe, J. M.; Engelkes, V. B.; Miller, L. L.; Frisbie, C. D. *J. Am. Chem. Soc.* **2002**, *124*, 11 268−11 269. (b) Wold, D. J.; Frisbie, C. D. *J. Am. Chem. Soc.* **2000**, *122*, 2970−2971. (c) Wold, D. J.; Frisbie, C. D. *J. Am. Chem. Soc.* **2001**, *123*, 5549−5556. (d) Cui, X. D.; Zarate, X.; Tomfohr, J.; Sankey, O. F.; Primak, A.; Moore, A. L.; Moore, T. A.; Gust, D.; Harris, G.; Lindsay, S. M. *Nanotechnology* **2002**, *13*, 5−11.

(10) (a) Holmlin, R. E.; Ismagilov, R. F.; Haag, R.; Mujica, V.; Ratner, M. A.; Rampi, M. A.; Whitesides, G. M. *Angew. Chem., Int. Ed.* **2001**, *40*, 2316−2320. (b) York, R. L.; Slowinski, K. *Journal of Electroanal. Chem.* **2003**, *550−551*, 327−336. (c) Moser, C. C.; Keske, J. M.; Warncke, K.; Farid, R. S.; Dutton, P. L. *Nature* **1992**, *355*, 796−802. (d) Beratan, D. N.; Onuchic, J. N.; Winkler, J. R.; Gray, H. B. *Science* **1992**, *258*, 1740−1747. (e) Li, T. T.; Weaver, M. J. *J. Am. Chem. Soc.* **1984**, *106*, 6107−6108. (f) Miller, C.; Cuendet, P.; Gratzel, M. *J. Phys. Chem.* **1991**, *95*, 877−881. (g) Yu, H.; Shao, H.; Luo, Y.; Zhang, H.; Liu, Z. F. *Langmuir* **1997**, *13*, 5774−5778.(h) Guo L. H.; Facci J. S.; G., M. *J. Phys. Chem.* **1995**, *99*, 8458−8462.

(11) Simmons J. G. *J. Appl. Phys.* **1963**, *34*, 1793−1803.

(12) (a) Holmlin, R. E.; Haag, R.; Chabinyc, M. L.; Ismagilov, R. F.; Cohen, A. E.; Terfort, A.; Rampi, M. A.; Whitesides, G. M. *J. Am. Chem. Soc.* **2001**, *123*, 5075−5085. (b) Mujica V., Ratner, M. A. *Chem. Phys.* **2001**, *264*, 365−370. (c) Wang W.; Lee T.; Reed M. A. *Physica E* **2003**, *19*, 117−125.

(13) Mujica, V.; Roitberg, A.; Ratner, M. A. *J. Chem. Phys.* **2000**, *112*, 6834−6839.

(14) (a) Davis, J. J.; Bruce, D.; Canters, G. W.; Crozier, J.; Hill, H. A. O. *Chem. Commun.* **2003**, 576−577. (b) Webb, M. A.; Loppnow, G. R. *J. Phys. Chem. B* **2002**, *106*, 2102−2108. (c) Adman, E. T. *Adv. Protein Chem.* **1991**, *42*, 145−197.

(15) Chi, Q.; Zhang, J. D.; Nielsen, J. U.; Friis, E. P.; Chorkendorff, I. B.; G. W. Canters; Andersen, J. E. T.; Ulstrup, J. *J. Am. Chem. Soc.* **2000**, *122*, 4047−4055.

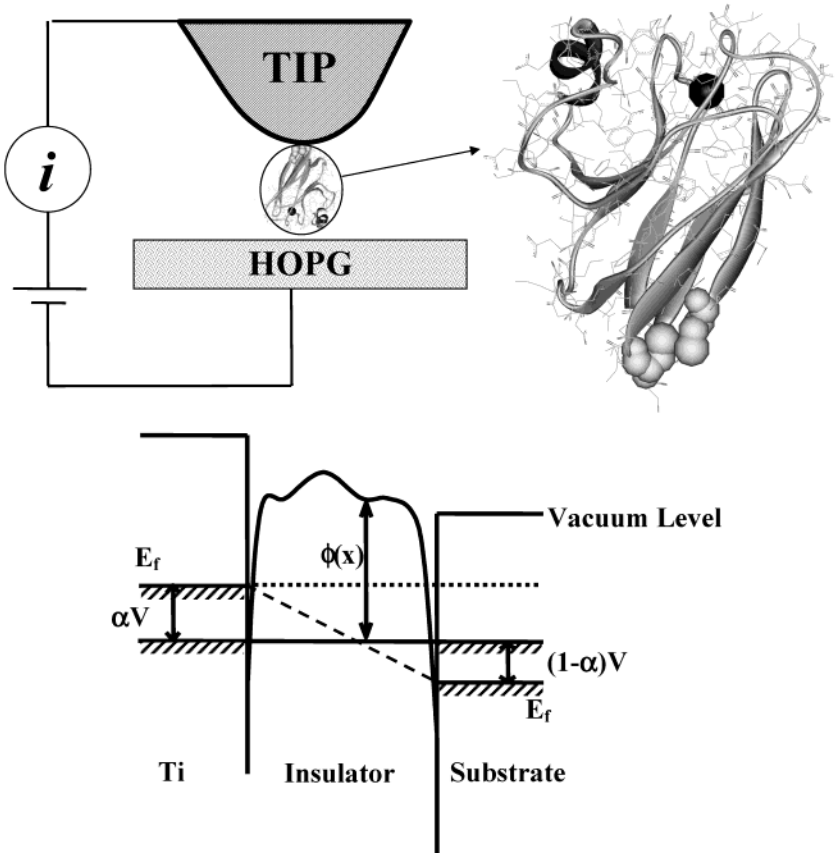

Figure 1. (a) Schematic representation of the conducting tip-oriented protein-HOPG junction, where a chemical bond is formed between tip and protein, whereas a physical contact between protein and HOPG. (b) Band diagram of the junction under application of bias.

the molecular level, its structural evolution during compressional deformation. Changes in the structure and properties of azurin with respect to compression in the simulations may be correlated with the observed force-conductance behavior of the protein.

Experimental Details

Materials. Azurin (*Pseudomonas aeruginosa* azurin wild-type) was kindly supplied by Professor Gerard Canters, Leiden Institute of Chemistry, Leiden. It was diluted in ca. 0.1 M acetate buffer (pH = 4.6, close to the protein isoelectric point) to form ca. 5 μM solutions characterized by UV−vis (Lambda 20, Perkin-Elmer Ltd.) with $\epsilon_{279} = 9800\ M^{-1}cm^{-1}$.

Conducting AFM Measurements. Gold-coated C-AFM probes (Si_3N_4 contact levers of 15 ± 5 nm tip radius, spring constant = 2.0 N/m, Mikromasch) were initially washed copiously with acetone, ethanol and deionized water (Millipore, 18.2 MΩ), and then modified with azurin by soaking in solution (~5 μM in azurin, acetate buffer) for at least 2 h. After incubation, the probes were rinsed copiously with deionized water to remove physically adsorbed material, blown dry with high purity argon and placed in the microscope. The tip was then brought into low force (<1 nN) contact with freshly cleaved highly oriented pyrolytic graphite (HOPG, Agar Scientific UK Ltd.) (Figure 1a). Electrical characterization was performed using a C-AFM (Pico AFM, Molecular Imaging) in contact mode with which I−V analyses can be performed independently of force feedback. 20 I−V curves were recorded for each force and experiments were carried out under ambient conditions (22 ± 2 °C, 40−50% humidity). Nonlinear least-squares fitting was performed with Origin 7.0 software and terminated at the point where a stable chi-squire value was achieved.

Methodology of Molecular Dynamics Simulations. Molecular dynamics (MD) simulations of azurin were performed in order to investigate its structural evolution under applied unidirectional compression. All simulations were performed under constant particle number, volume and temperature (NVT) conditions using GROMACS version 3.1.4.[16] The GROMOS96 force field parameters were employed for all simulations. Time steps of 2 fs were used.[16] A cutoff of 1.0 nm was employed for both van der Waals' and electrostatic interactions and bond lengths were constrained via the LINCS algorithm.[17] The protein was coupled to a temperature bath at 300 K and analyses of MD trajectories were performed using GROMACS.[18] Visualization of system geometries and evaluation of protein secondary structure were performed using the program VMD.[19]

Results and Discussion

Tunneling Current Expression. In the present study, the protein electron-transfer medium is sandwiched between a

(16) (a) Spoel, D. v. d.; Buuren, A. R. v.; Apol, E.; Meulenhoff, P. J.; Tieleman, D. P.; Sijbers, A. L. T. M.; Hess, B.; Feenstra, K. A.; Lindahl, E.; Drunen, R. v.; Berendsen, H. J. C. *Gromacs User Manual version 3.1*; Nijenborgh 4, 9747 AG Groningen, The Netherlands. Internet: www.gromacs.org, 2002. (b) Gunsteren, W. F. v.; Kruger, P.; Billeter, S. R.; Mark, A. E.; Eising, A. A.; Scott, W. R. P.; Huneberger, P. H.; Tironi, I. G. *Biomolecular Simulation: The GROMOS96 Manual and User Guide*; Biomos & Hochschulverlag AG an der ETH Zurich, Groningen & Zurich, 1996.
(17) Hess, B.; Bekker, H.; Berendsen, H. J. C.; Fraaije, J. G. E. M. *J. Comput. Chem* **1997**, *18*, 1463−1472.
(18) Berendsen, H. J. C.; Postma, J. P. M.; Gunsteren, W. F. v.; DiNola, A.; Haak, J. R. *J. Chem. Phys.* **1984**, *81*, 3684−3690.
(19) Humphrey, W.; Dalke, A.; Schulten, K. *J. Mol. Graphics* **1996**, *14*, 33−38.

conducting AFM tip and planar substrate. Within such a configuration current flow will be observed through the protein if (i) the electrons in the electrodes have enough thermal energy to surmount the potential barrier and flow into the molecular obitals or (ii) the barrier width is sufficiently thin to permit penetration by tunneling. In view of the relative magnitudes of thermal energy and tunnel barrier, room temperature thermal contributions to conductance can be, to a first approximation, ignored. The tunnel current density observed across two electrodes separated by a thin insulting film has been provided by Simmons (eqs 1 and 2) and is depicted diagrammatically in Figure 1b, where symmetrical (equivalent) electrodes are associated with a bias division factor of 0.5. This model can be applied to any potential barrier fitting the Wentzel−Kramers−Brillouin (WKB)[5] approximation with a mean barrier height, φ_0. Alternatively, if the I−V characteristics of a tunnel junction are known, the mean barrier height and barrier length can be determined by theoretical fitting. A modified form of eq 1 and (2) have been recently proposed by Whitesides[12] and Lindsay.[20] In short, this modification replaces the mass of the tunneling electrons in eq 2 by the effective mass, m^*. The Simmons model (eqs 1 and 2) and its simple derivatives predict a symmetric I−V spectrum and require further modification if accurate predictions of current flow at higher force are to be made (see below).[12,20]

In consideration of the junction characterized in this study (Figure 1a), where the material and geometry of the two electrodes are dissimilar, and the orientated protein is both asymmetric and coupled covalently to one electrode,[14] a more reasonable treatment is to divide the voltage drop into two nonequivalent components as follows.[21]

$$V = \alpha V + (1 - \alpha)V \tag{4}$$

where αV is the elevated potential of tip (see Figure 1b), and $(1-\alpha)V$ the reduced potential of substrate. Under such conditions, the net current density should be expressed as

$$i = \frac{e^2}{2\pi h L^2}\{(\varphi_0 - \alpha V)\exp[-K(\varphi_0 - \alpha V)^{1/2}] - [\varphi_0 + (1 - \alpha)V]\exp[-K(\varphi_0 + (1 - \alpha)V)^{1/2}]\} \tag{5}$$

In a "symmetric situation" where the fraction of the bias division, α, is equal to 1/2, eq 5 simplifies to the original Simmons expression (eq 1).

Metalloprotein I−V Spectra. Typical I−V curves at small (6.0 nN) and moderate (32.0 nN) force are given in Figure 2. Despite the presence of a redox-accessible copper state, no resonances are observed within the swept bias range. An asymmetric feature associated with more rapid increase in current at positive tip bias than at negative, can be identified in the experimental data (open circles). At 6.0 nN, the current at +0.6 V (8.9×10^{-11} A) is, for example, 4.9% higher than that at −0.6 V (-8.5×10^{-11} A) (Figure 2a). This asymmetry, which has been observed in studies carried out with other organic monolayers (such as alkane thiol SAMs), is slight at low force where the symmetric Simmons model can be thus applied with reasonable accuracy.[9,10,12] At higher junction forces, however, I−V asymmetries become more pronounced; at 32.0 nN, for example, the current at +0.6 V (7.1×10^{-9} A) is 84% higher than that at −0.6 V (-3.9×10^{-9} A). Under such conditions, experimental data is not accurately predicted by eq 1.

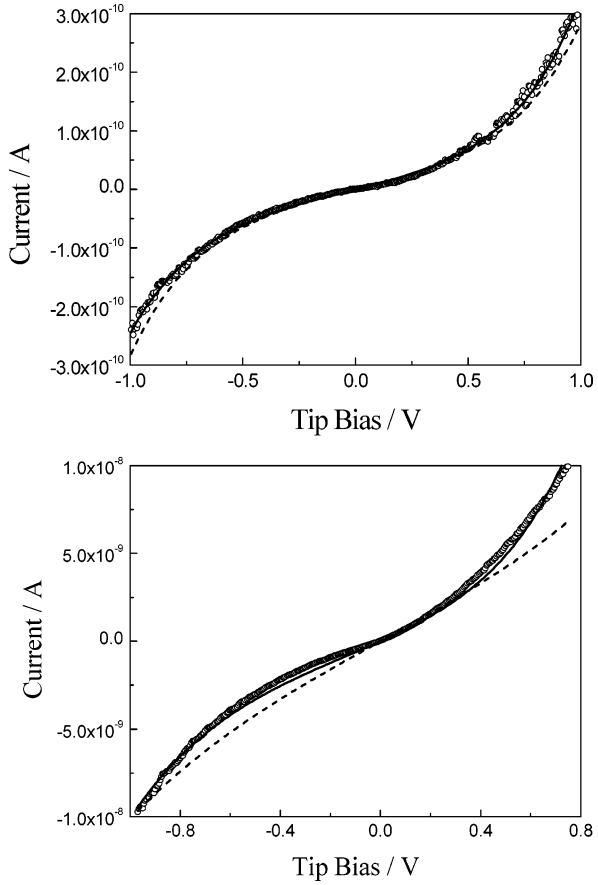

Figure 2. Typical asymmetric I−V features of the Metal-Protein-HOPG junction. (a) force 6.0 nN; (b) force 32.0 nN. (open circle) Experimental data; (dotted line) simulated by Simmons model; (solid line) simulated by modified Simmons model. Currents are -8.49×10^{-11} A (−0.6 V) and 8.91×10^{-11} A (+0.6 V), and -3.89×10^{-9} A (−0.6 V) and 7.14×10^{-9} A (+0.6 V) corresponding to 6.0 nN and 32.0 nN, respectively (see text).

Table 1. Comparison of Nonlinear Least Squares Fitting by Original Simmons Model and Modified Simmons Model

force/nN	parameters	Simmons model	modified Simmons model
6.0	φ_0 (eV)	1.11 ± 0.01	1.105 ± 0.006
	L (nm)	1.17 ± 0.01	1.17 ± 0.004
	α		0.525 ± 0.001
	χ^2 value	2.2×10^{-22}	3.3×10^{-23}
32.0	φ_0 (eV)	1.31 ± 0.14	0.706 ± 0.007
	L (nm)	0.64 ± 0.04	0.89 ± 0.006
	α		0.583 ± 0.001
	χ^2 value	1.2×10^{-18}	9.29×10^{-20}

Comparative symmetric (eq 1) and asymmetric (eq 5) simulations are shown in Figure 2 and summarized in Table 1. At low force the (original) Simmons equation tracks the experimental data well and allows the generation of self-consistent tunnel barrier and length parameters. At higher compressional force the predictions of eqs 1 and 5 deviate markedly; barrier length and height variance is an order of magnitude greater with eq 1. The modified model, however,

(20) Cui, X. D.; Primak, A.; Zarate, X.; Tomfohr, J.; Sankey, O. F.; Moore, A. L.; Moore, T. A.; Gust, D.; Nagahara, L. A.; Lindsay, S. M. *J. Phys. Chem. B* **2002**, *106*, 8609−8614.
(21) Tian, W.; Datta, S.; Hong, S.; Reifenberger, R.; Henderson, J. I.; Kubiak, C. P. *J. Chem. Phys.* **1998**, *109*, 2874−2882.

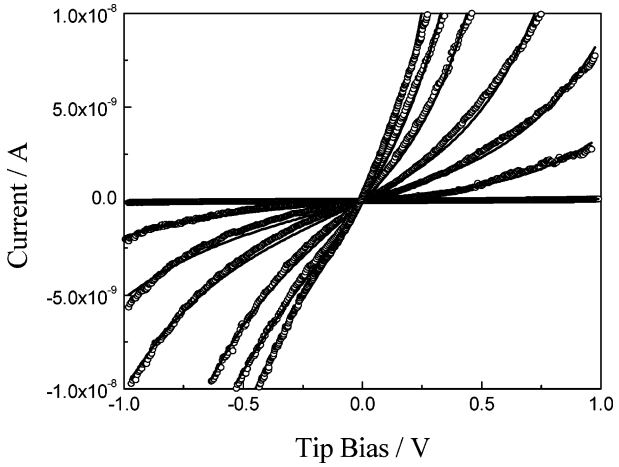

Figure 3. Typical set I−V curves for the forces of 10.4, 24.5, 30.4, 37.3, 43.6, 50.6, and 56.4 nN. (open circle) Experimental data; (solid line) simulated by modified Simmons model.

continues to fit the observed data accurately and appears, then, to be a more appropriate description of the metalloprotein junction.

In simulating the experimental results using eq 5, the contact area was assumed to be that defined by the diameter (3 nm) of the metalloprotein. Though it is impossible to deconvolute the contributions of increased contact area under increasing force from the pressure-dependent protein electron-transfer characteristics, the effects of variable area have minimal (linear) impact on the current in comparison to distance and barrier height (exponential) (eqs 1 and 4). The reliability of using a fixed contact area can be inspected by fitting the raw data (open circles in Figure 2a) to eq 1 across a range of contact areas. A 10-fold increase in area (3.1×10^{-18} to 3.1×10^{-17} m^2) produces < 10% change in calculated barrier heights and lengths (the change in parameter, χ, being defined here by $(\chi_i - \chi_{ave})/\chi_{ave}$, where χ_{ave} is its mean value). Uncertainty in contact area, then, does not impede the reliable determination of these parameters (this is an important conclusion in the subsequent analysis of protein mechanics − see below).

Force Dependence of Tunneling Conductance. The effects of junction force on azurin I−V characteristics is depicted in Figure 3. The (predictable) compression of protein on increasing force results in increased current flow across the junction; initially slow, then rising rapidly at higher force. These observations have been made with similarly confined compressible molecules such as, alkanethiol SAMs.[9] Three-variable (barrier height (φ_0), length (L), and fraction of bias division (α)) simulations fit the experimental data well across the entire force regime depicted (solid lines). The tunnel parameters obtained by fitting are given in Figure 4. The fitted tunnel barrier, φ_0, was observed to monotonically decrease with increasing force. Predictably, the barrier length, L, initially decreases, but is then predicted to increase (Figure 4b, open circles). Though fitting is still good, the variance of L at higher force clearly indicates a failure of this model to predict realistic variations (an increase in L at high compression is nonsensical).

It is instructive to consider the nature of the molecular perturbation responsible for this observed abrupt change in junction characteristics at higher force. In doing this we have used an atom packing density model in which the structural space present within the three-dimensional fold is compressible

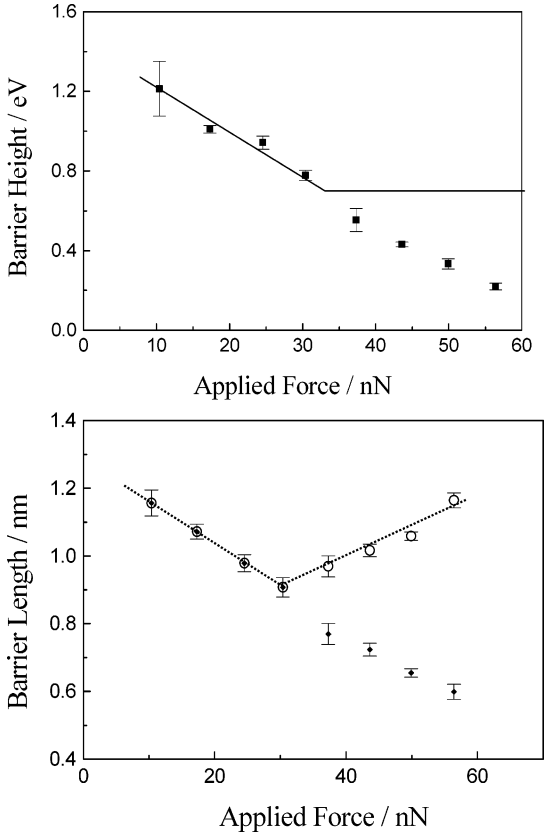

Figure 4. Force dependence of (a) barrier height (φ_0) and (b) barrier width (L) obtained by least-squares fitting by eq 5. The tunnel lengths obtained by three-variable fitting are denoted by the open circles. The corresponding force of the switch point was averaged to be 30 ± 5 nN (5 samples). The barrier height (φ_0) is taken to be constant after this switch point (see text for details) as shown by solid line in (a). The simulated barrier width (L) using the corrected (φ_0) is given by the solid diamonds in (b).

within the tunnel junction (Figure 5). Dutton has considered the effects of atomic packing on the ability of a protein matrix to mediate electron transfer, and given an empirical expression to account for structure-dependent variations of the tunneling coefficient, β[1]

$$\beta = \rho \times 0.9\ \text{Å}^{-1} + (1 - \rho) \times 2.8\ \text{Å}^{-1} \qquad (6)$$

In principle, the atom packing density, ρ, can range from 1, corresponding to a fully packed medium ($\beta \approx 0.9$ Å^{-1}), to a value of 0, corresponding to the interstitial space in the protein structure ($\beta = 2.8$ Å^{-1}).[9,10,22] β and φ_0 are correlated through following equation as derived from eq 1 and (2)

$$\beta = 1.025\ \varphi_0^{1/2} \qquad (7)$$

while L is in angstroms, φ_0 in electronvolts, and β in Å^{-1}.[10,11,20] We suggest here that increasing the compressional force within the tunnel junction leads to an increase in atom packing density, ρ, to 1 (with a corresponding decrease in β and φ_0). The limit of force-induced atom density increase is provided by the repulsive forces which develop rapidly as interatomic separations are reduced and, ultimately, will lead to protein deformation in the surface plane. At this stage, ρ and β (or φ_0) are maximized and minimized respectively (eqs 6 and 7).

(22) Miller, C.; Gratzel, M. *J. Phys. Chem.* **1991**, *95*, 5225−5233.

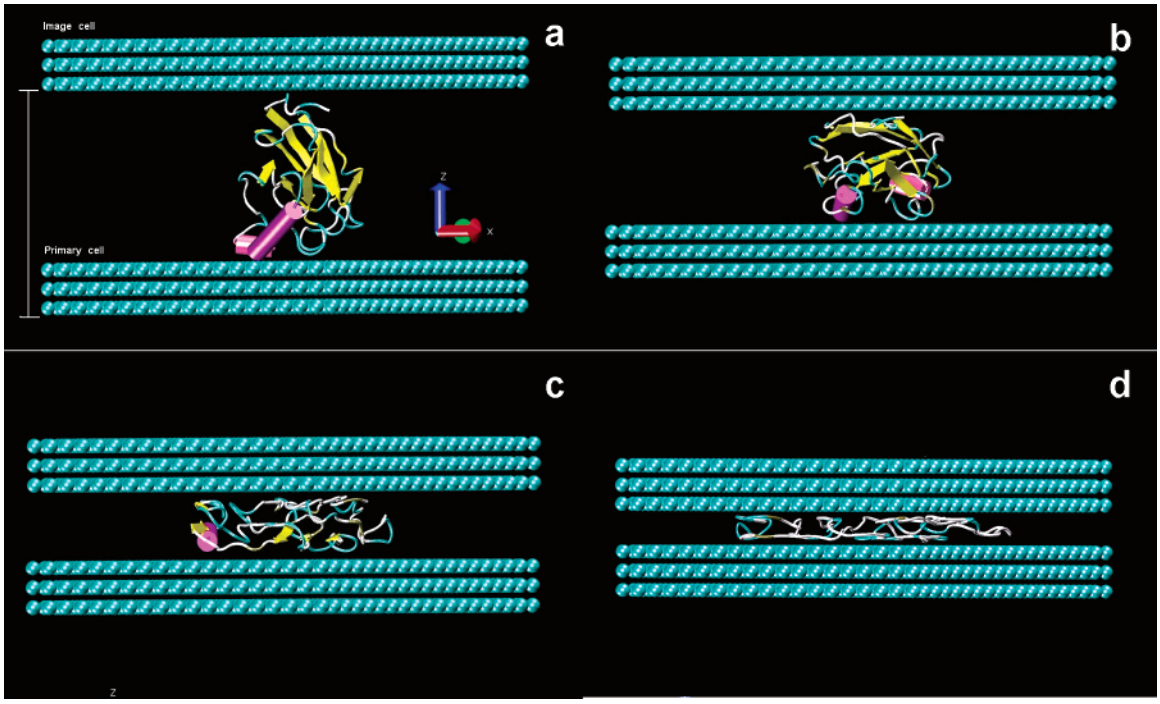

Figure 5. Structure evolution of the azurin molecule on a surface constructed from united-atom CH_4 molecules at interfacial separation distances of (a) 4.0 nm, (b) 2.7 nm, (c) 1.7 nm, and (d) 1.0 nm.

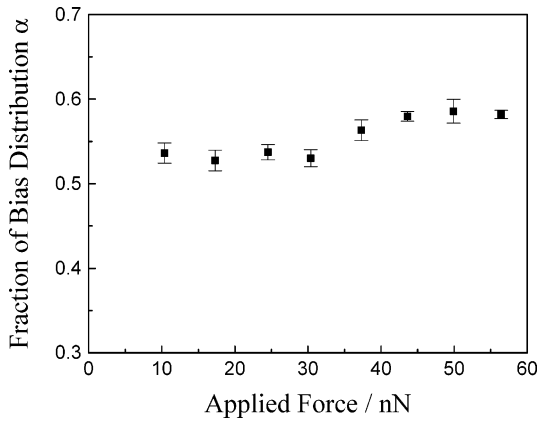

Figure 6. Fraction of the bias distribution, α, obtained by fitting with a modified Simmons model, as a function of applied force.

For azurin, the force at which this switch in electronic characteristics is observed was found, averaged over five samples, to be 30 ± 5 nN. Beyond this point, the three-variable fitting fails. Reliable fits to data can be maintained at high force through the simple assumption of continued linear decrease of L at constant φ_0 (solid line in Figure 4a), that is by reducing the fitting algorithm to two variables (solid dots in Figure 4b). The (thereafter fixed) barrier height at this point was averaged to be 0.76 ± 0.15 eV, which corresponds to 0.89 ± 0.09 $Å^{-1}$. It should be noted that this value is in good agreement with β at $\rho \approx 1$ (eq 6) for the closely packed system, further suggesting the attainment of maximum atom packing density.[9,10]

The variance of the derived bias division, α, with force, at fixed φ_0 is given in Figure 6. In all cases derived values of α are larger than 0.5 meaning the Fermi level potential shift at the tip is more significant than that at the substrate. Though similar observations have been recently reported by Majda et al. in transport studies across alkanethiol bilayer junctions,[23] an accurate (physical) interpretation of this remains currently difficult.

Protein Mechanics in the Junction. From the fitting-derived linear decrease in tunnel length with force, one can estimate the mechanical properties of the protein using the stress−strain relation. Specifically, the Young's modulus (E) can be obtained by following equation

$$E = \sigma/\epsilon \tag{8}$$

where stress, σ, is defined as applied force (F) divided by contact area (A), and strain, ϵ, as deformation (ΔL) of protein divided by the initial length (L_0) at *time zero* (the point at which electrical contact to the protein is established). A and L_0, then, must initially be determined, though it is important to note that L_0 as determined from the described conductance measurements has, in essence, no physical meaning (since no conductance data is derived on the uncompressed protein). As discussed earlier, the protein cross section is assumed to constitute the contact area. The tunnel length at *time zero*, L_0, can be derived by extrapolation (Figure 4b).

The azurin Young's modulus derived from the slope of the subsequently generated stress−strain plot (Figure 7), is 1.4 ± 0.1 × 10^{10} N/m^2. This value is within an order of magnitude of bulk determinations made in viscoelastic or acoustic experiments and close to determinations made on, for example, alkanethiol SAMs on gold.[24,25] One may, on the basis of atom density,

(23) Galperin, M.; Nitzan, A.; Sek, S.; Majda, M. *J. Electroanal. Chem.* **2003**, *550*−*551*, 337−350.
(24) (a) Rosser, R. W.; Schrag, J. L.; Ferry, F. D.; Greaser, M. *Macromolecules* **1977**, *10*, 978−980. (b) Tamura, Y.; Suzuki, N.; Mikashi, K. *Biophys. J.* **1993**, *65*, 1899−1905.
(25) (a) Nelles, G.; Schönherr, H.; Jaschke, M.; Wolf, H.; Schaub. M.; Küther, J.; Tremel, W.; Bamberg, E.; Ringsdorf, H.; Butt, H. *Langmuir* **1998**, *14*, 808−815. (b) Thomas, R. C.; Houston, J. E.; Michalske, T. A.; Crooks, R. M. *Science* **1993**, *259*, 1883−1885. (c) Kiridena, W.; Jain, V.; Kuo, P.; Liu, G. *Surf. Interface Anal.* **1997**, *25*, 383−389.

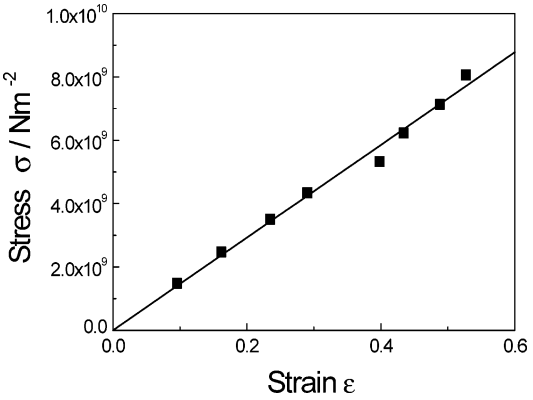

Figure 7. Stress ($\sigma = F/A$) strain ($\epsilon = (L_0 - L)/L_0$) relation of azurin.

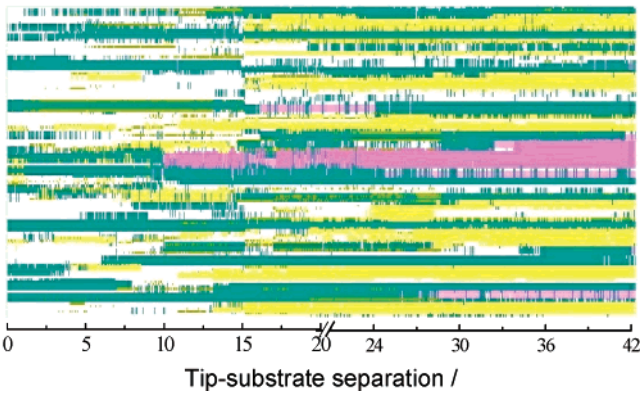

Figure 8. Secondary structure as a function of interfacial separation (nm). Colors represent secondary structural elements as follows: pink = α-helix, yellow = β-strand, aqua = loop, white = disordered.

expect the resistance to compression of a protein in which density is maximized to be comparable to that of a saturated alkyl.

The stress−strain relationship depicted in Figure 7 is almost linear and goes through the coordinate origin. In this sense, the protein compression process seems to be 'elastic'.[26] Conductance experiments, however, strongly suggested that the compressed metalloprotein fails to return to its original vertical dimensions (I−V behavior) on reduction of imposed force. The processes of compression and recovery are driven by different forces; the former by an externally imposed mechanical force, and the latter by van der Waals' forces among the peptide chains.[27] Similar irreversible protein deformation has been also observed in a micro slide contact measurement, where a hysteresis was observed for the first and subsequent compressions.[28] These observations, then, are consistent with plastic protein deformation. The "relaxation effects" associated with the removal of all compressional force on the protein are currently under further investigation.

Molecular Dynamics Simulation of Compressional Protein Deformation. Atomistic simulations of azurin were performed in order to investigate structural evolution under unidirectional compression. The surface and AFM tip were modeled as two nonpenetrative surfaces comprising of united-atom methane molecules, separated by the protein. Tip geometry and composition are not explicitly modeled within this scheme. It is assumed that the force exerted by the tip on the protein is due entirely to steric repulsion, and the former may therefore be approximated as a collection of inert, hard-sphere-like CH_4 molecules. In view of the relative dimensions of tip apex and protein (the tip radius of curvature significantly exceeds the protein diameter), the region of the tip in direct contact with the protein is approximated as being flat. Further details of the model applied in the present simulations are provided in the Supporting Information.

The structures of azurin at interfacial separations of 4.2, 2.7, 1.7 and 1.0 nm are shown in Figures 5a−d using standard "cartoon" representations of the protein backbone, in which α-helices are represented by cylinders and β-strands by arrows. The secondary structure of the protein (calculated using DSSP) for all residues as a function of interfacial separation is shown in Figure 8.[29] Examination of the tertiary and secondary structures with compression shows that, although the overall shape of the protein undergoes distortion ("flattening") upon contact with both surfaces, the major secondary structure elements are maintained even under significant compression, with unfolding of these elements only occurring upon decrease of the separation distance to approximately 1.7 nm (as illustrated in Figure 8). This is in qualitative agreement with several previous simulations of globular proteins (such as bovine pancreatic trypsin inhibitor (BPTI) and β-amylase) under applied isotropic pressures, where it has been found that no significant unfolding is observed even under high pressures within time scales of approximately 1 ns.[30] It is also reminiscent of the overall pattern of unfolding of proteins during simulated AFM stretching, where secondary structures persist despite the application of high pulling forces; see, for example, Lu et al.[31] Additionally, structural elements such as the α-helix and the β-strands (labeled as A and B respectively in Figure 5a) initially lie at approximately 45° and 80° to the surface plane, respectively, but lie parallel to the surface at moderate compressions rather than unfold, suggesting that they are stable under applied force up to a certain point. At an interfacial separation of approximately 1.4 nm (close to the van der Waals' diameter of an α-helix), essentially all secondary structure has been lost due to excessive compressive force. A plot of the radius of gyration (R_g) of the protein with respect to interfacial separation (see Figure 9) shows that the protein remains in a compact, folded state in the range of 4.2 nm (a distance greater than the folded protein diameter)[32] down to 2.5 nm, but rapidly unfolds below this distance. We note that there is a slight decrease in the radius with increasing compression within 4.2 and 3.0 nm, which suggests that the protein packing increases with applied force within this range, as discussed below.

To obtain an estimate of the degree of atomic packing within azurin under varying degrees of compression, the trajectory-averaged number density profiles of the protein at each

(26) Timoshenko, S. P.; Goodier, J. N. *Theory of Elasticity*; McGraw-Hill: New York, 1970.
(27) Bao, G. J. *Mech. Phys. Solids* **2002**, *50*, 2237−2274.
(28) Singh-Zocchi, M.; Hanne, J.; Zocchi, G. *Biophys. J.* **2002**, *83*, 2211−2218.
(29) Karbsch, W.; Sander, C. *Biopolymers* **1983**, *22*, 2577−2637.
(30) (a) Marchi, M.; Akasaka, K. *J. Phys. Chem.* **2001**, *105*, 711−714. (b) Paci, E.; Marchi, M. *Proc. Natl. Acad. Sci. U.S.A.* **1996**, *93*, 11 609−11 614.
(31) Lu, H.; Isralewitz, B.; Krammer, A.; Vogel, V.; Schulten, K. *Biophysical J.* **1998**, *75*, 662−671.
(32) (a) Nar, H.; Messerschmidt, A.; Huber, R.; Kamp, M. v. d.; Canters, G. W. *J. Mol. Biol.* **1991**, *221*, 761−764. (b) Berman, H. M.; Westbrook, J.; Feng, Z.; Gilliland, G.; Bhat, T. N.; Weissig, H.; Shindyalov, I. N.; Bourne, P. E. *Nucleic Acids Res.* **2000**, *28*, 235−242.
(33) Arcangeli, C.; Cannistraro, S. *Biophys. Chem.* **2001**, *92*, 183−199.
(34) Tobias, D. J.; Mar, W.; Blasie, J. K.; Klein, M. L. *Biophys. J.* **1996**, *71*, 2933−2941.

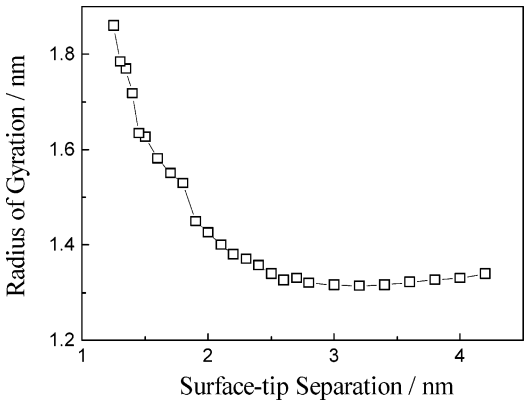

Figure 9. Trajectory-averaged radius of gyration (R_g in nm) of the azurin protein plotted with respect to interfacial separation (nm).

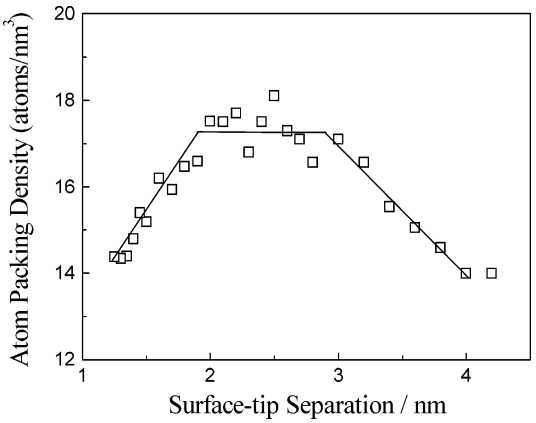

Figure 10. Maximum *x*-axis number density (atoms/nm^3) of azurin plotted with respect to interfacial separation (nm).

compression step were plotted with respect to the *x* axis (as defined in Figure 5a). Data acquired from *y*-axis profiles yielded the same results and revealed the same trends. In this scheme, the simulation cell is divided into 10 slices of equal width, parallel to the *z* and *y*-axes and perpendicular to the *x*-axis. The number of atoms per unit volume for each slice is subsequently determined and plotted as a function of the *x* coordinates. The maximum value of the number density ρ_{max} for each compression step was plotted with respect to interfacial separation distance, as shown in Figure 10.

[This value was chosen for several reasons. The *x* coordinate where the density reaches a maximum value corresponds to the region at which the protein completely spans the space between the two surfaces. The density in this region is therefore likely to be an important influence on the tunneling coefficient. Additionally, ρ_{max} is more sensitive to changes in interfacial separation compared to the density in other regions, and therefore allows a clear trend to be established.]

As shown in Figure 10, ρ_{max} increases linearly with compression down to approximately 3.0 nm of interfacial separation, reaches a maximum between 3.0 and 2.0 nm, and subsequently decreases with decreasing distance. This appears to be consistent with the secondary structure map (Figure 8) and R_g plot (Figure 9) discussed above, and suggests that while the protein fold is sustained (i.e., at interfacial separations from 4.2 to 2.9 nm), increasing applied force results initially in enhanced packing density. However, within the 2.9−1.9 nm range, the combined effects of applied compression (which tend to increase atom packing) and in-plane deformations due to protein distortion (which tend to decrease atom packing) result in a roughly constant value of packing density with further compression (note that within this range, the protein fold is still maintained, as shown in Figure 8). Below 1.9 nm, excessive compression results in unfolding of the protein and loss of secondary structural elements, causing significantly enhanced in-plane deformations which result in lowered packing density.

Taking into account the observed secondary structure, R_g and ρ_{max} changes with respect to compression obtained from the present simulations, a qualitative mechanism may be proposed for the experimentally observed behavior of the tunneling barrier height and length as a function of applied force (Figure 4 and text in section 3.3). For the following discussion, it should be noted that values of the tip−surface separations in the MD simulations do not correspond quantitatively to the transport-derived experimentally fitted values. For example, the "switch point" (the point at which atom packing density reaches a maximum and ceases to increase with compression) was determined to be 0.9 nm from theoretical fitting to experimental I−V data, but it is taken to be approximately 2.9 nm in the MD simulations (Figure 10). As discussed below, however, trends observed from both approaches are qualitatively consistent; the MD simulation predictions are accordingly useful in aiding our interpretation of experimentally observed changes in molecular transport with compression.

Initially, the protein undergoes deformation as compressive force is applied, resulting in approximately monotonic enhancement in atomic packing with increasing force, with retention of the major secondary structural elements. The approximately monotonic increase in ρ_{max} correlates qualitatively with the monotonic decrease of tunneling barrier height observed experimentally in transport data. However, beyond the "switch point" (corresponding to 30 nN force in the experiment, and around 2.9 nm separation in the MD simulation), ρ_{max} reaches a plateau. This is manifested in the experiment as a roughly constant value of tunneling coefficient with applied force beyond the switch point. In the simulations, compression below 1.7−2.0 nm causes protein unfolding and significant in-plane deformation, resulting in an overall decrease in packing density. Although this may, in principle, result in increase in the protein tunneling coefficient with compression, this effect is not resolved in the current work. This may be due to either outweighing increases in current flow at the onset of direct tip-to-surface tunneling at low tip−surface separations or the avoidance of such a compressional regime even at the maximal forces at which current flow was reproducibly measured.

Conclusions

A full physical understanding of protein-mediated electron transfer is of considerable importance in not only the design of the protein-based electronic devices but also in attaining an adequate level of understanding of their behavior. In this study, the tunneling characteristics of the blue copper metalloprotein, azurin have been studied at the molecular level through the use of conducting AFM. By modifying the metallic probe by chemisorption of solvent-exposed disulfide moieties, stable tunnel junctions can be formed which can be subsequently scrutinized under controllable conditions. The experimental data has been considered in terms of a nonresonant charge-transfer

process in which the protein matrix is modeled as a uniform tunnel barrier. Though the simple Simmons model provides a reasonable qualitative description of experimental data, a modification taking into account the asymmetries present in "real" tunnel junctions is necessary if accurate simulations are to be attainable. Though an asymmetry in bias devision is an empirical requirement if good fits to experimental data are to be obtained, the physical basis of this is as yet unclear and the subject of further investigation. The force modulation of I−V behavior was interpreted in terms of protein geometric change and accompanying modulations of barrier height and length. Tunnel barrier determinations at low and high molecular compression correlate reasonably well with the results of previous "bulk-scale" biochemical and electroanalytical/tunneling analyses on proteins and saturated hydrocarbons, respectively. From tunneling and molecular dynamics simulations the plastic compression of protein per unit applied vertical force has allowed a determination of Youngs' modulus.

Molecular dynamics simulations were performed in order to examine the effects of compression on azurin, with particular focus on changes in protein structure and packing density. The packing density was found to increase monotonically with compression up to approximately 3.0 nm, corresponding to the "switch point" observed in experiments, and reach a roughly constant value between 3.0 and 2.0 nm. This is consistent with the experimental behavior of tunneling coefficient with respect to applied force as well as the applicability of an atom packing density model of electron tunneling in proteins, even at the molecular level.

Although these simulation results correlate well with the experimental transport data, it will be necessary in further work to address the approximations inherent in the tip-protein-surface model discussed in this manuscript. Current work in this area includes studies of the behavior and the effects of hydration water on the protein under compression. Further work will also focus on the construction of more realistic models of the AFM tip and graphitic substrate and parametrization of copper−protein, tip−protein, protein−surface and tip−surface interaction potentials.

Acknowledgment. The authors wish to acknowledge the EPSRC and Interdisciplinary Research Collaboration (IRC) in Bionanotechnology for financial support.

Supporting Information Available: Supplementary section on molecular dynamics simulations. This material is available free of charge via the Internet at http://pubs.acs.org.

JA039392A